Superconductivity and short-range order in metallic glasses $Fe_xNi_{1-x}Zr_2$

J. Lefebvre, M. Hilke, and Z. Altounian
Department of Physics, McGill University, Montréal, Canada H3A 2T8
(Received 3 December 2008; revised manuscript received 4 March 2009; published 26 May 2009)

In amorphous superconductors, superconducting and vortex-pinning properties are strongly linked to the absence of long-range order. Consequently, superconductivity and vortex phases can be studied to probe the underlying microstructure and order of the material. This is done here from resistance and local magnetization measurements in the superconducting state of $Fe_xNi_{1-x}Zr_2$ metallic glasses with $0 \leq x \leq 0.6$. First, we present typical superconducting properties such as the critical temperature and fields and their dependence on Fe content in these alloys. Then, the observations of peculiar clockwise hysteresis loops, wide double-step transitions, and large magnetization fluctuations in glasses containing a large amount of Fe are analyzed to reveal a change in short-range order with Fe content. The results further shed light on our understanding of the interplay among superconducting coherence lengths, material microstructure, and pinning and how they can influence superconducting transitions in transport measurements.

DOI: 10.1103/PhysRevB.79.184525 PACS number(s): 74.25.Fy, 74.25.Ha, 74.81.Bd

I. INTRODUCTION

Since the synthesis of the first amorphous alloy superconductors by vapor deposition by Bückel and Hilsch[1] in 1954, and the following, fabricated in the mid-1970s by electron-beam evaporation by Collver and Hammond,[2] our understanding of superconducting phenomenon in this new class of superconductors has greatly evolved. Although these first attempts at making amorphous alloys were plagued by the inconvenient instability of the amorphous phase at room temperature, they have served to expose the differences between superconductivity in amorphous materials and in their crystalline counterpart. Nowadays, several techniques based on the rapid cooling of the melt are used to fabricate stable amorphous alloys and the past 25 years have seen the publication of many studies about superconductivity in such metallic glasses, especially those composed of transition-metal alloys.[3–11] These studies have, among other things, discussed the importance of including effects due to spin fluctuations in the predictions of T_c, especially in alloys containing Ni, Co, or Fe. Additionally, they have identified the important role played by microstructure and short-range order (SRO) in amorphous materials, and, for instance, how it is influenced by thermal relaxation. Since microstructure critically depends on the fabrication process and the melt-cooling rate, values for different superconducting characteristics such as the critical temperature T_c from different laboratories for the same alloy composition often vary significantly. Another particularity of superconductivity in amorphous alloys which has been largely investigated is the linearity of the temperature dependence of the upper critical field over an extended range of temperature ($\gtrsim 0.6\ T_c$) in the vicinity of T_c.[3,4,12,13] Such a linear $B_{c2}(T)$, inconsistent with the predictions of Werthamer *et al.*[14] and Maki,[15] is not observed in crystalline superconductors nor in microcrystalline transition-metal alloys[3,4,12] but seems to be general for this class of material. This extended range of linearity along with enhanced $B_{c2}(T)$ has been suggested to arise due to the presence of inhomogeneities on the range of the Ginzburg-Landau coherence length ξ_{GL}.[16]

Vortices in type-II superconductors can typically also reveal important information about material structure. In particular, defects and dislocations provide pinning sites which prevent vortex movement and enhance pinning. On the contrary, the absence of long-range order in amorphous materials greatly decreases the pinning properties. Moreover, several superconducting properties, for instance, the shape and width of the B_{c2} transition or magnetization hysteresis loops are direct consequences of the homogeneity of the material and its flux-trapping capacities. Also, the effectiveness of superconductivity as a probe of amorphous-material inhomogeneity, such as caused by phase separation or the presence of microcrystallites, evidenced by enhanced $B_{c2}(T)$ and paraconductivity, has already been well established.[17–19]

Binary and pseudobinary compounds composed of the early transition (ET) metal Zr and late transition (LT) metal Cu, Ni, Co, and Fe in the form LT_xET_{1-x} and $(LT_x^aLT_{1-x}^b)_yET_{1-y}$ have shown excellent glass-forming abilities over a wide compositional range.[5,9,11,20,21] In the past, it has been assumed that SRO in the pseudobinary compound $Fe_xNi_{1-x}Zr_2$ would not be affected by the Fe content x because Fe and Ni have very similar atomic diameters.[21] The homogeneity of the amorphous phase has also been verified by x-ray diffraction and electron-beam microprobe analysis.[20] In this paper, we study $Fe_xNi_{1-x}Zr_2$ superconducting glasses with $0 \leq x \leq 0.6$ based on electric transport and local magnetization measurements. The high purity and the amorphous nature of these alloys, conferring them extremely weak-pinning properties, have previously allowed us to investigate transversely ordered dynamic-vortex phases.[22–24] Here, we exploit the relationship between vortex pinning and material structure to reveal a change in SRO in this glass series. This conclusion is reached based on the observation of peculiar hysteresis loops and magnetization fluctuations in alloys containing a relatively large amount of Fe. Superconducting properties of the metallic glasses and their dependence on the Fe content x are also presented.

II. EXPERIMENTAL METHODS

Alloy buttons are prepared by arc-melting appropriate amounts of the elemental constituents Fe (99.9%), Ni

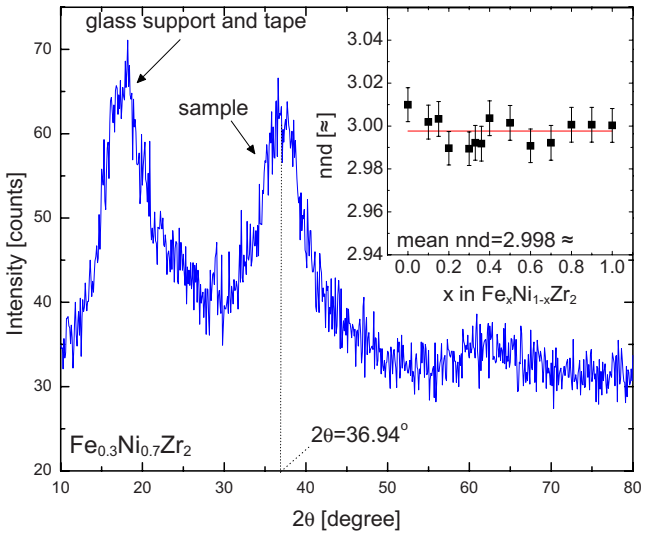

FIG. 1. (Color online) X-ray diffraction spectrum of $Fe_{0.3}Ni_{0.7}Zr_2$ measured with Cu $K\alpha$ radiation. The first peak is from diffraction from the glass support. The second peak is from diffraction from the sample. The position of this peak is determined from a Gaussian fit and the value is used in Ehrenfest's relation to obtain nnd. Inset: near-neighbor distance for each alloy. The line shows the mean nnd for the whole alloy series.

(99.999%), and Zr (99.95%) under Ti-gettered argon atmosphere in order to avoid oxidation. The buttons are remelted three times to ensure homogeneity. Amorphous ribbons are then prepared by melt spinning the alloy buttons. Melt spinning is performed in 40 kPa helium onto a copper wheel spinning at 50 m/s which ensures that the rapid cooling rate of 10^5-10^6 K/s necessary for the formation of the amorphous phase is attained. The absence of crystallinity was confirmed from the absence of constructive Bragg peaks in x-ray Cu $K\alpha$ diffraction (Fig. 1). Indium contacts are soldered to the samples to permit electrical measurements in the standard four-probe technique. Resistance measurements are performed with a resistance bridge providing ac current at 15.9 Hz in a ^{3}He refrigerator. The use of a dilution refrigerator was also required for measurements of the superconducting properties of $Fe_{0.6}Ni_{0.4}Zr_2$ due to the low T_c below 0.3 K. In both the ^{3}He system and the dilution refrigerator a superconducting magnet with field capability up to 9 T was used. The temperature is determined from calibrated Cernox and RuO resistors.

Glass structure

The question of the nature of the ordering in the amorphous phase in the pseudobinary $Fe_xNi_{1-x}Zr_2$ series deserves particular attention. In the past, it has been tacitly assumed that the SRO characterizing the amorphous structure of these alloys does not change upon substitution of Ni for Fe because these atoms have very similar sizes. Thereupon, various studies assuming constant glass structure in these and similar glasses were undertaken[20,21,25–27] to study the dependence of certain effects on glass composition, independently of structural-change effects. Constant geometrical short-range order (GSRO) across the series of alloys, mainly provided by constant near-neighbor distances (nnd's), is readily verified from the position of the primary diffraction peak θ in x-ray diffraction data and from the Ehrenfest relation[28,29] $\bar{r}=0.6148\lambda/\sin\theta$; the mean near-neighbor distance $\bar{r}$ is evaluated, as shown in the inset of Fig. 1, using $\lambda=1.5405$ Å, the wavelength of Cu $K\alpha$ radiation. As observed, the nnd in this alloy series is indeed constant with a mean nnd of 2.998 Å, which confirms constant GSRO in these alloys. This however does not necessarily imply that SRO is constant: since Fe and Ni have different electronic structures, chemical short-range order (CSRO), pertaining mainly to the atomic species of near neighbors and their arrangement, cannot be assumed to remain constant. This question was previously investigated in these alloys using Mössbauer spectroscopy[21] but no change in SRO with x could be evidenced outside experimental uncertainties. However, the existence of a transition in SRO with x would not be too surprising since it is known that the atomic arrangement in amorphous materials resembles closely that of the first crystallization products,[30,31] and while the first crystallization products of $NiZr_2$ have a body-centered-tetragonal structure, those of $FeZr_2$ have a face-centered-cubic structure. Therefore, one can wonder what is the atomic arrangement or if phase separation takes place in intermediate compositional range $Fe_xNi_{1-x}Zr_2$ with x between 0.1 and 0.9. As will be shown and discussed later in this paper, some results about superconductivity in this alloy series point to a transition in SRO and complement well other results published in Ref. 32.

III. RESULTS

A. Superconducting properties

Initial interest in the study of superconductivity in the metallic glasses $Fe_xNi_{1-x}Zr_2$ was based on the assumed constant glass structure. Indeed, this would permit a study of the dependence of superconductivity on alloy composition and more specifically the influence of spin fluctuations, independently of structure-dependent effects.[20] Spin fluctuations, induced by the presence of magnetic atoms in the alloys, tend to demote superconductivity by causing spin flips which break Cooper pairs. Consequently, one expects a suppression of the typical parameters characterizing superconductivity, such as critical temperature T_c and upper critical field B_{c2} with increasing Fe content. Such a behavior is witnessed in these alloys, as shown in Fig. 2(a) and 2(b). As can be seen, T_c of these alloys varies from 2.6 to about 0.2 K with increasing Fe content from $x=0$ to 0.6. T_c is determined from resistance measurements in zero-magnetic field and defined when the resistance reaches half the normal-state value, i.e., at $R_n/2$. The values reported for the alloys are from several measurements on up to five different samples of each alloy composition. Among samples of the same alloy, typical T_c variations observed are smaller than 0.1 K; such a distribution of T_c's in an alloy is expected and inherent to the fabrication process. Indeed, the copper wheel used for melt spinning becomes hotter in the process such that not the whole ribbon is cooled at exactly the same rate and the beginning of the ribbon can show significant differences in microstructure

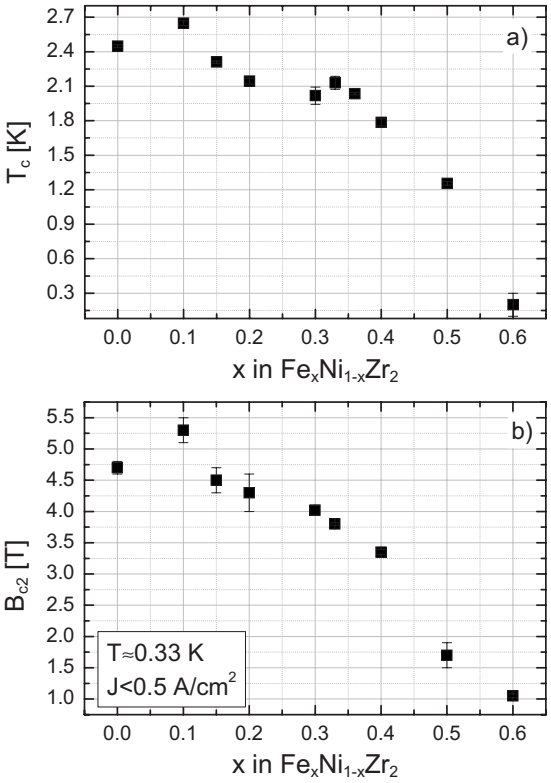

FIG. 2. (a) Critical temperature and (b) upper critical field as a function of Fe content x in $Fe_xNi_{1-x}Zr_2$. Error bars are statistical. For $x=0.6$, $T<100$ mK during measurement of B_{c2}.

compared to the end of the ribbon; these differences are then reflected in superconducting properties. Typically, annealing the samples at a temperature close to the glass transition temperature will remove these differences in microstructure along the length of the ribbon. However, doing this, we nevertheless get a distribution of T_c's in a single alloy. The T_c's reported here are generally lower than those reported 15 years ago in Ref. 20 on these same alloys; a discrepancy attributed to increased structural relaxation which takes place in alloys stored at room temperature.[5] A T_c higher than obtained here has also been previously reported in $Fe_{0.5}Ni_{0.5}Zr_2$ in Ref. 8 but values from different laboratories are hardly comparable because properties of metallic glasses critically depend on fabrication conditions. We also observe an augmentation of T_c from $x=0$ to 0.1 which could result from an enhancement of the density of states at the Fermi level in $Fe_{0.1}Ni_{0.9}Zr_2$ compared to $NiZr_2$; this idea is supported by evidence from ultraviolet photoemission spectroscopy on binary alloys of Fe-Zr and Ni-Zr which have shown that the Fe d band lies closer to the Fermi level than the Ni d band.[33]

Similarly, the upper critical field B_{c2} [Fig. 2(b)] was determined from resistance measurements performed as a function of magnetic field at a fixed temperature between 0.33 and 0.35 K for the $0\leq x\leq 0.5$ alloys using a low driving current density $J<0.5$ A/cm^2. For the $x=0.6$ alloy, the temperature was below 0.1 K. The values reported are from a few measurements on different samples. We define the B_{c2} transition at $R_n/2$ because, as will be demonstrated in Sec. III B, some of our samples are inhomogeneous, most likely composed of two slightly different amorphous phases. This definition of B_{c2} then reflects some average of this parameter for the two phases. In addition, it will be shown later that the B_{c2} transition exhibits large clockwise hysteresis loops in the $x=0.5$ and $x=0.6$ alloys; in these cases, the value of B_{c2} reported corresponds to the mean value obtained from up- and down-going field sweeps, i.e., $(B_{c2}^{\mathrm{down}}-B_{c2}^{\mathrm{up}})/2$. It should also be noted that this B_{c2}, measured from transport measurements, is expected to differ from the thermodynamic B_{c2}, especially in inhomogeneous samples, because in the former case, as soon as a superconducting percolation path exists across the sample, the measurements reflect superconductivity along this path, although nonsuperconducting regions (or regions having different, less favorable for current transport, superconducting properties) might still exist. This can be contrasted to global magnetization measurements for instance, in which the measurements reflect the average properties of the whole sample. It is found that B_{c2} decreases from 5.3 to 1 T with increasing Fe content and, just like T_c, B_{c2} increases for the alloy $x=0.1$ compared to $x=0$, again pointing to some promotion of superconductivity by the introduction of a small amount of Fe. Except in $x=0.5$, these values are slightly larger than the Clogston limit[34] $B_p(0)=\frac{\Delta(0)}{\sqrt{2}\mu_B}$ from 4.55 T in $x=0$ to 0.52 T in $x=0.6$, which indicates that paramagnetic effects do not limit B_{c2} in these alloys. The presumed inhomogeneity of alloys $x=0.5$ might be responsible to some extent for the measured B_{c2} lower than B_p.

In Table I, we report various physical and superconducting parameters of the $Fe_xNi_{1-x}Zr_2$ metallic glasses. Spin fluctuations at temperatures above the superconducting transition have been studies before in these alloys,[20] and this is a systematic study of superconducting properties for different alloy compositions. The normal-state resistivity ρ_n is calculated from resistance measurements performed at room temperature on long ribbons (>30 cm) such as to minimize geometry-dependent effects. ρ_n of the order 1.68 $\mu\Omega$ m is obtained for all alloys; these values are close to the values reported for similar alloys.[5,8,9,11] Since ρ_n is related to the GSRO, the constant ρ_n throughout this composition range brings further confirmation of the constant GSRO. The slope of the upper critical field as a function of temperature close to T_c, $\frac{dB_{c2}}{dT}|_{T_c}$, is determined from a single set of measurements of the resistance as a function of temperature at different magnetic fields. We obtain $\frac{dB_{c2}}{dT}|_{T_c}\simeq -2.4$ T/K as typical in amorphous alloys (see, for instance, Refs. 11, 13, and 35). We also report values for the penetration depth $\lambda(0)$, the coherence length $\xi_G(0)$ (analogous to BCS ξ_0 but including correction due to short mean free path, as indicated by Gor'kov[36,37]), and the Ginzburg-Landau coherence length $\xi_{\mathrm{GL}}(0)$ and the GL parameter κ evaluated from expressions for superconductors in the dirty limit.[38] In $NiZr_2$, we obtain $\lambda(0)=0.87$ μm and $\xi_{\mathrm{GL}}(0)\simeq 8.1$ nm; these values generally increase with Fe content to reach 3.04 μm and 16.2 nm, respectively, in $x=0.6$. This means that the vortex size and core increase substantially when going from $x=0$ to $x=0.6$. This should have important effects on vortex-pinning properties and vortex-vortex interactions. A systematic study of vortex phases depending on Fe content in these metallic

TABLE I. Some measured and calculated physical and superconducting parameters.

Alloy	ρ_n ($\mu\Omega$ m)	$\frac{dB_{c2}}{dT}\|_{T_c}$ [a] (T/K)	$\lambda(0)$ [b] (μm)	$\xi_G(0)$ [c] (nm)	$\xi_{GL}(0)$ [d] (nm)	κ [e]	l [f] (Å)	$B_{c1}(0)$ [g] (mT)
$NiZr_2$	1.68 ± 0.02	-3.0 ± 0.2	$0.87\pm5\%$	$6.7\pm20\%$	$8.1\pm4\%$	$79\pm20\%$	$2.7\pm40\%$	0.47 ± 0.05
$Fe_{0.1}Ni_{0.9}Zr_2$	1.68 ± 0.01	-2.2 ± 0.4	0.84	7.5	8.0	68	2.7	0.59 ± 0.05
$Fe_{0.15}Ni_{0.85}Zr_2$	1.62 ± 0.08	-2.8 ± 0.1	0.88	7.2	8.3	75	2.9	N.A.
$Fe_{0.2}Ni_{0.8}Zr_2$	1.69 ± 0.01	-2.4 ± 0.4	0.93	8.0	8.2	71	2.8	0.59 ± 0.04
$Fe_{0.3}Ni_{0.7}Zr_2$	1.75 ± 0.02	-2.8 ± 0.1	0.98	7.6	8.8	78	2.7	0.60 ± 0.06
$Fe_{0.33}Ni_{0.67}Zr_2$	1.84 ± 0.08	-3.2 ± 0.1 [h]	0.98	7.0	8.7	86	2.6	N.A.
$Fe_{0.36}Ni_{0.64}Zr_2$	1.72 ± 0.05	-3.2 ± 0.1	0.97	7.1	N. A.	83	2.7	N.A.
$Fe_{0.4}Ni_{0.6}Zr_2$	1.70 ± 0.02	-2.6 ± 0.2	1.02	8.4	9.6	74	2.8	0.69 ± 0.06
$Fe_{0.5}Ni_{0.5}Zr_2$	1.69 ± 0.01	-2.3 ± 0.1 [h]	1.22	10.1	12.3	70	2.8	0.34 ± 0.04
$Fe_{0.6}Ni_{0.4}Zr_2$	1.67 ± 0.01	N.A.	3.04	N. A.	16.2	N. A.	2.9	N.A.

[a]The errors reported on $\frac{dB_{c2}}{dT}|_{T_c}$ consider the maximum and minimum slopes that could be obtained considering systematic errors on T and B_{c2}.

[b]Obtained from $\lambda(0)=1.05\times10^{-3}(\frac{\rho_n}{T_c})^{1/2}$.

[c]From $\xi_G(0)=1.81\times10^{-8}[T_c|\frac{dB_{c2}}{dT}|_{T_c}]^{-1/2}$.

[d]From $\xi_{GL}(0)=[\frac{\Phi_0}{2\pi B_{c2}(0)}]^{1/2}$. $B_{c2}(0)$ is obtained from the extrapolation to $T=0$ of fits to the WHHM theory (Ref. 14) of $B_{c2}(T)$ data.

[e]From $\kappa=3.54\times10^4[\rho_n|\frac{dB_{c2}}{dT}|_{T_c}]^{1/2}$.

[f]The percentage error on l is computed by considerering the effect on l of using a free-electronlike Fermi-surface ratio $S/S_F=1$.

[g]Obtained from fits to $B_{c1}=B_{c1}(0)[1-(T/T_c)^4]$ of B_{c1} data from local-magnetization measurements between $T=0.35$ K and T_c (Ref. 32).

[h]Determined from resistance measurements as a function of magnetic field sweeps at different temperatures.

glasses would probably yield interesting results. The GL parameter κ is around 80 in these alloys, thus confirming that they are hard type-II superconductors. The mean free path is evaluated from

$$l=(3\pi^2)^{1/3}\left[e^2\rho_n\left(n_e^{2/3}\frac{S}{S_F}\right)\right]^{-1}, \quad (1)$$

where n_e is the free-electron density and S/S_F is the ratio of the area of the free Fermi surface to that of a free-electron gas of density n_e. Both these quantities are estimated as follows: n_e is the ratio of the average number of electrons per atom outside closed shells to the atomic volume, i.e., $n_e=\langle\frac{e}{a}\rangle V_0^{-1}$. In this manner we have $2.9\times10^{29}\leq n_e\leq3.2\times10^{29}$ m^{-3} with n_e decreasing with increasing Fe content. We also use $S/S_F=0.6$ as in Ref. 11; although if we were to use $S/S_F=1$ as for a free-electron Fermi surface the value of l would not change by 1 order of magnitude. As a result, we obtain $l\simeq2.8$ Å which is very close to the mean interatomic distance (nnd=2.998 Å) in these amorphous alloys. As a result of the short mean free path, we obtain a dirtiness parameter[47] $\xi_G(0)/l$ above 20. This means that electrons undergo many scattering events within the size of the coherence length and effectively confirms that these amorphous alloys are in the dirty limit. We also evaluate the electron-phonon coupling parameter $\lambda_{ep}\simeq0.6$ using the McMillan equation[39]

$$\lambda_{ep}=\frac{1.04+\mu^*\ln(\Theta_D/1.45\,T_c)}{(1-0.62\mu^*)\ln(\Theta_D/1.45\,T_c)-1.04}, \quad (2)$$

where we have used the Coulomb interaction parameter $\mu^*=0.13$ for polyvalent transition metals[39] and the Debye temperature $\Theta_D=192.5$ K as evaluated for $NiZr_2$ according to Ref. 5. This λ_{ep} makes the $Fe_xNi_{1-x}Zr_2$ metallic glasses in the weak- to intermediate-coupling regime. Diffuse electron scattering in amorphous alloys enhances electron-phonon interactions above values of their crystalline counterpart.

B. Structure inhomogeneity and CSRO

Several physical properties of amorphous alloys depend on CSRO, for instance, the Curie temperature, the temperature coefficient of resistivity, and superconducting properties. In the case of superconductivity, this is because structural order directly influences the electron-phonon coupling parameter, resulting in a modification of T_c for instance. Structural order can also influence superconductivity by acting on vortex-pin interactions, in particular, defects, impurities, and inhomogeneities, and can thus define the current-carrying capacities of the superconductor. For instance, it is the absence of long-range order in amorphous alloys which mainly determine their weak vortex-pinning properties. The effects of structural inhomogeneity are also commonly observed in superconducting properties, such as wide B_{c2} or T_c transitions.[18,40] In this section, we discuss some evidences of structural inhomogeneity in the $Fe_xNi_{1-x}Zr_2$ with a large Fe content $0.4\leq x\leq0.6$ obtained from resistance and magnetization measurements in the superconducting state. As will be shown, the results lead us to believe that in glasses with $x\neq0$ and $x\neq1$, phase separation into Ni-rich and Fe-rich regions having SRO characteristic of $NiZr_2$ and $FeZr_2$, respectively, takes place.

1. Width of transition

A first obvious sign of the growth of structural inhomogeneity with Fe content in these alloys is provided by an

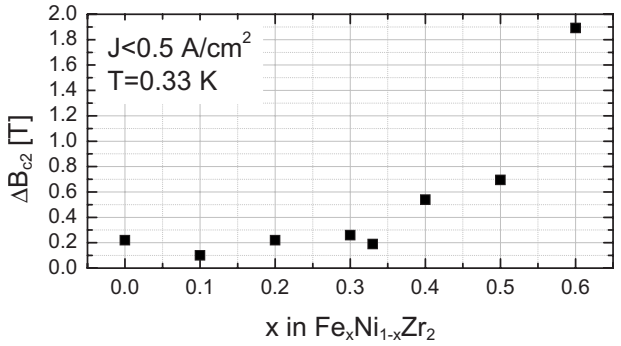

FIG. 3. Width of the B_{c2} transition for different $Fe_xNi_{1-x}Zr_2$ alloys. In $x=0.6$, this includes both transitions 1 and 2.

increase in the width of the B_{c2} transition $\Delta B_{c2} \equiv B(0.9R_n) - B(0.1R_n)$, as shown in Fig. 3. A double-step transition is even observed in some of the alloys $x=0.5$ and 0.6 (Fig. 4): an indisputable indication of a two-phase material.

2. Clockwise hysteresis

In type-II superconductors, the B_{c2} transition between the normal state and the superconducting state often exhibits hysteresis due to Joule heating where more power is dissipated in the normal state than in the superconducting state and to flux pinning and trapping. The hysteresis loop is then counterclockwise, i.e., the B_{c2} transition is higher upon increasing the magnetic field than when decreasing it. These types of hysteresis loops are observed here for alloys with $0 \leq x \leq 0.4$ (Fig. 4) in which the B_{c2} transition is slightly lower upon decreasing (dotted lines) the magnetic field than upon increasing (solid lines) it. This can be contrasted to the large clockwise hysteresis loops seen at B_{c2} in the alloys $x=0.5$ and $x=0.6$. All the $x=0.5$ samples measured (7) show this wide clockwise hysteresis loop, although only two of them show the double-step transition. The only $x=0.6$ sample measured shows a very broad B_{c2} transition about 2 T wide including the two steps. A reversal of the hysteresis loop direction in $x=0.6$ is observed between transitions 1 and 2 as identified in the figure; the uppermost transition exhibits the usual counterclockwise hysteresis loops.

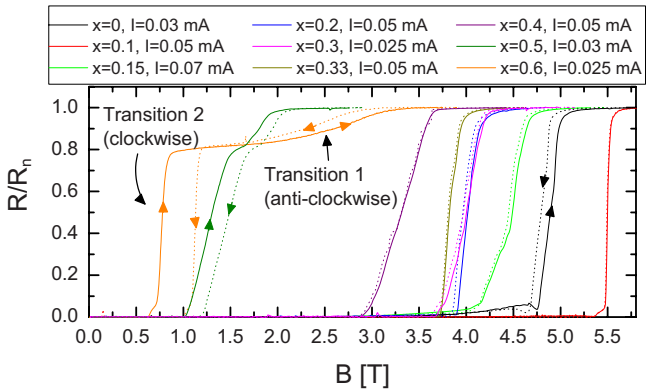

FIG. 4. (Color online) Resistance as a function of magnetic field for different alloys. The solid and dotted lines are for increasing and decreasing B sweep, respectively. The magnetic field was swept at a rate of 0.0147 T/s and the temperature was below 0.35 K.

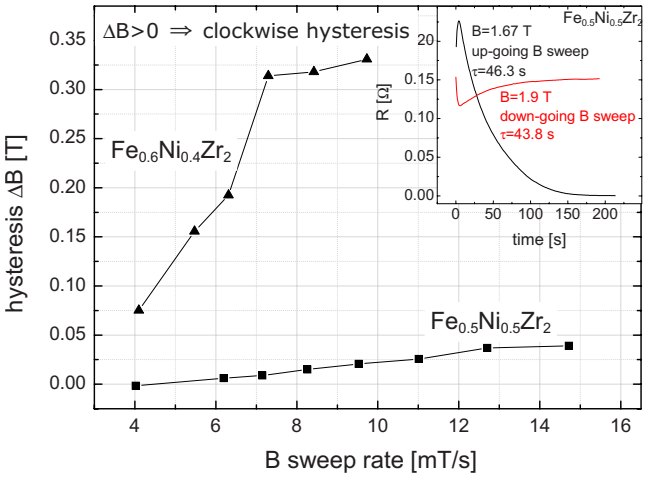

FIG. 5. (Color online) Width of clockwise hysteresis loop as a function of magnetic field sweep rate. ΔB is defined as the difference in magnetic field when the resistance reaches 0.5 R_n for down-going (B_{c2}^{down}) and up-going (B_{c2}^{up}) field sweep, i.e., $\Delta B = (B_{c2}^{down} - B_{c2}^{up})/2$. Only the lowermost transition (transition 2) is considered here in $x=0.6$. For $Fe_{0.5}Ni_{0.5}Zr_2$, $T=0.34$ K and $I=30$ μA. For $Fe_{0.6}Ni_{0.4}Zr_2$, $T<0.1$ K and $I=5$ μA. The line is a guide for the eye. Inset: resistance as a function of time when B field sweep is paused in the middle of the B_{c2} transition. $I=0.03$ mA and $T=0.33$ K.

We have resistively measured the B_{c2} transition in $x=0.5$ and 0.6 for different B sweep rates. The results, presented in Fig. 5, show an increase in the size of the hysteresis loops with increasing B sweep rate. This dependence on sweep rate provides evidence that a dynamical process, such as vortex motion, is at the origin of the hysteresis loops. This is further supported by the data shown in the inset of Fig. 5, which shows the resistance as a function of time when the magnetic field sweep is paused in the middle of the B_{c2} transition during an increasing and a decreasing magnetic field sweep. Time $t=0$ corresponds to the moment when the field sweep is paused. As can be seen, after $t=0$ the resistance initially keeps increasing (decreasing) over a short period of time for increasing (decreasing) B sweep but it eventually reverses and decreases (increases) back to zero (a value close to what it was before the sweep was paused). Fitting these time dependences to an exponential obtains a time constant τ of 46.3 and 43.8 s for the up- and down-going field sweeps respectively, indicating a slow dynamical process. On the contrary to what is observed in magnetic field sweeps, no clockwise hysteresis loops are observed in temperature sweeps across T_c in a fixed magnetic field (data not shown). This brings further confirmation that the clockwise hysteresis loops are governed by a dynamical process involving vortex motion rather than some phase transition.

In the literature, simulations of V-I characteristics in superconductors with inhomogeneous pinning potentials show clockwise hysteresis loops.[41,42] Such hysteresis loops result from dynamical effects and interplay between vortex trapping in the strong- and weak-pinning regions. As such, the size (or width) of the hysteresis loops is seen to depend on the sweep rate of the external variable with respect to which the loop is observed; in Refs. 41 and 42, this is the driving

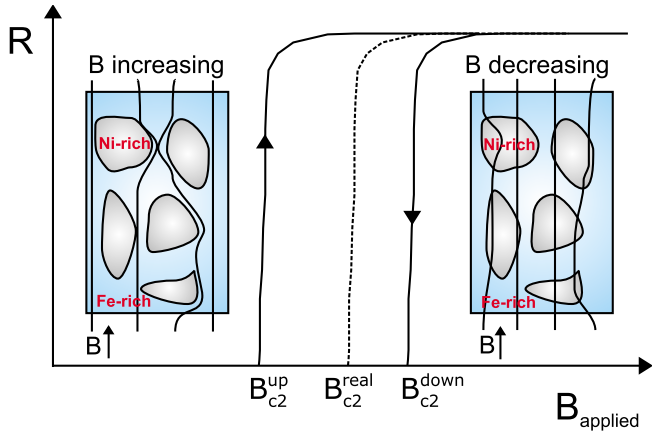

FIG. 6. (Color online) Schematic representation of the resistive B_{c2} transition for up- and down-going field sweeps with corresponding inhomogeneous vortex distribution in the superconductor. For increasing B field, more vortices pass through the weakly pinned Fe-rich phase, avoiding the Ni-rich regions and the B_{c2}^{up} transition appears lower than it should be if the fluxes were homogeneously distributed in the whole sample (B_{c2}^{real}). The inverse phenomena occur upon decreasing B with vortices tending to remain in the more strongly pinned Ni-rich clusters such that B_{c2}^{down} appears higher than B_{c2}^{real}.

current and the driving force. As is the case in our B-induced hysteresis loops, the size of the loops increases in Refs. 41 and 42 for faster driving force-sweep speeds.

Based on these simulation results and our data, we propose that the anomalous clockwise hysteresis loops observed at the B_{c2} transition here arise due to the presence of inhomogeneities, some having stronger and weaker pinning properties, and thus resulting in an inhomogeneous distribution of vortices in the superconductors. If we picture the sample as being composed of regions having stronger pinning properties than the surrounding medium and if this medium also provides the connected path across the sample, we can explain the appearance of clockwise hysteresis loops in magnetic field sweeps and their absence in temperature sweeps as follows: as B is increased from 0, vortices will first penetrate in the main connected phase since it has the lowest pinning properties and thus a lower energy barrier against flux entry. Then, due to the elasticity of the vortex lattice, as the magnetic field is increased further it will be energetically more favorable for the vortices to bend around the strong-pinning regions[43] and remain in the main connected phase. This will result in an inhomogeneous distribution of magnetic flux in the superconductor with a larger flux density being present in the main connected phase, i.e., the phase of which the superconducting properties are measured in resistance measurements. As a consequence, the B_{c2} transition appears lower upon increasing the magnetic field than it would be if the fluxes were homogeneously distributed throughout the sample. A schematic representation of this process is presented in Fig. 6. On the contrary, upon decreasing the magnetic field from above B_{c2}, fluxes tend to stay trapped in the strong-pinning regions but easily leave the weak-pinning main phase which again results in an inhomogeneous distribution of vortices in the sample, but this time with the lowest vortex density in the main phase. This results in a resistively measured B_{c2} transition upon decreasing the magnetic field that is higher than it should be. These two processes then result in clockwise hysteresis loops. Similar phenomena have been observed previously in granular superconductors[43–45] and inhomogeneous superconductors.[17,41,42]

This model explains why we witness an increase in the width of hysteresis loops with increasing B sweep rate: for slower sweep rate the vortices have more time to penetrate into the strong-pinning grains or to diffuse into the weak-pinning regions upon increasing and decreasing the magnetic field before the measurement is taken. Therefore, after we apply a certain field, and by the time we take the measurement, the vortex distribution has reached a more homogeneous configuration for slower sweep speeds and results in smaller hysteresis loops. A similar observation was made by Liu *et al.*[41] and Xu *et al.*[42] from numerical simulations and experimental measurements of flux creep in a superconductor with inhomogeneous pinning properties. In these cases however, the size of hysteresis loops was observed to increase with increasing driving current and driving force-sweep rate, but the result is equivalent: changing the sweep rate amounts to changing the observation time window. Namely, for a slow sweep rate, our observation window is too late to observe the large inhomogeneity in the flux distribution.

The results presented in the inset of Fig. 5 also lead to the conclusion that the vortex distribution is inhomogeneous in these alloys. For instance, when the field is paused in an increasing magnetic field sweep, the resistance initially keeps increasing because fluxes easily and rapidly enter the weak-pinning phase; however it eventually starts decreasing as no more fluxes are added (paused B) and the fluxes in the weakly pinned regions start to diffuse in the strong-pinning grains, thus yielding a more homogeneous vortex distribution which brings the observed B_{c2} transition closer to the real value. The opposite takes place when the field is paused in a decreasing B sweep; the resistance change over approximately the same period of time is however smaller and indicates that the flux distribution is more homogeneous at B_{c2} in a decreasing B sweep than in an increasing one.

According to this model, no clockwise hysteresis loops are expected in temperature sweeps performed in a fixed external field because, in this case, the vortex density is fixed and its distribution across the sample remains the same as the temperature is swept up and down.

3. Magnetization fluctuations

As described in detail elsewhere,[32,46] local magnetization measurements were performed on these metallic glasses ($0 \leq x \leq 0.5$) using a two-dimensional electron-gas Hall probe. Fluctuations in the magnetization, increasing with Fe content, were observed and analyzed to reveal the presence of large vortex clusters of over 70 vortices and size over 10 μm in the superconductors with a large Fe content $x > 0.4$ (see Fig. 7). It was also argued that the vortex bundles likely arise in these alloys because they are composed of two phases having different SROs and thus different pinning properties. In all alloys with $x > 0$ phase separation takes

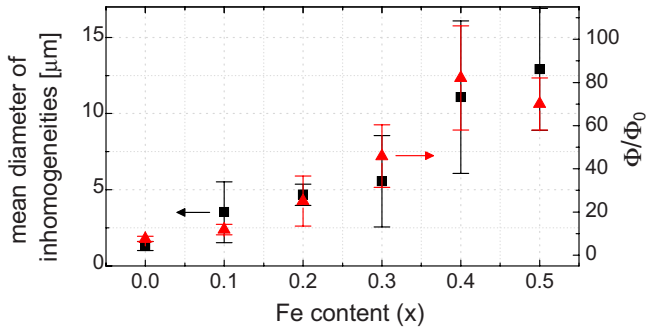

FIG. 7. (Color online) Black squares: mean diameter of inhomogeneities evaluated from the relative size of magnetization fluctuations as described in Ref. 32. Red triangles: number of vortices in clusters related to the magnetization fluctuations.

place, as both Fe-rich and Ni-rich phases exist, as evidenced from larger magnetization fluctuations in $x=0.1$ compared to $x=0$, but the regions of the Fe-rich phase become larger and more numerous in $x>0.4$. These results point to the existence of a structural phase transition close to $x=0.4$ with alloys $x<0.4$ having mostly $NiZr_2$-like SRO and alloys with $x>0.4$ having mostly $FeZr_2$-like SRO.

Summarizing the results presented in this section, many evidences indicate phase separation into Fe-rich and Ni-rich regions in the $Fe_xNi_{1-x}Zr_2$ metallic glasses, particularly, in the compositions with a large Fe content. Both the gradual increase in the width of the B_{c2} transition (Fig. 3) and increasing size of magnetization fluctuations revealing the presence of large vortex clusters (Fig. 7) with x point to an augmentation of the presence of inhomogeneities, most likely Fe-rich regions. The very broad ΔB_{c2}, the double-step transition, and the appearance of large clockwise hysteresis loops in $x=0.5$ and 0.6 further support this idea and provide indication that Fe-rich regions have become critically large in these alloys but some Ni-rich regions remain. It should be noted that the differences in glass structure between the Fe-rich and Ni-rich phases must be very subtle because no evidence of a two-phase material is seen in x-ray diffraction (Fig. 1) and has not been seen either in isomer shift[21] and electron-beam microprobe analyses.[20] Considering these results, it should be noted that the T_c and the B_{c2} values reported in Fig. 2, as well as the various parameters of Table I reflect an average of these parameters in the Fe-rich and the Ni-rich phases.

IV. CONCLUSIONS

In summary, we have presented the Fe content dependence of superconductivity in the metallic glasses $Fe_xNi_{1-x}Zr_2$. As expected due to the augmentation of spin fluctuations, T_c and B_{c2} decrease with increasing x. This decrease becomes more pronounced in $x=0.5$ and $x=0.6$; but in the light of the results presented here, which suggests that these glasses have a two-phase structure, it is hard to decouple how much of the increased T_c and B_{c2} depression rate is due to spin fluctuations and how much is due to the different SROs. Although the discovery of phase separation in these alloys does not allow for a precise study of spin-fluctuation effects on superconductivity independently of structure-dependent contributions, important progress was made in our understanding of short-range order in this amorphous alloy series. While we have shown that GSRO remains constant across the series as expected, numerous evidences, such as an increase in B_{c2} transition width with x, the appearance of double-step transitions and large clockwise hysteresis loops, and the observation of large fluctuations in magnetization in high Fe containing alloys, point to the conclusion that two phases having different CSROs exist in these alloys. According to these results, a Fe-rich phase having SRO resembling that of $FeZr_2$ appears with a Fe content as low as $x=0.1$ but becomes critical around $x=0.5$, where important effects on superconductivity are witnessed. These results evidence that the assumption of constant glass structure in these metallic glasses is wrong and should, on the contrary, be considered carefully, especially in structure-dependent measurements, such as the magnetic properties of superconductors, in which the small vortex core has proved to be highly sensitive to the microstructure of the material.

[1] W. Bückel and R. Hilsch, Z. Phys. **138**, 109 (1954).
[2] M. M. Collver and R. H. Hammond, Phys. Rev. Lett. **30**, 92 (1973).
[3] W. L. Johnson and S. J. Poon, J. Appl. Phys. **46**, 1787 (1975).
[4] W. L. Johnson, S. J. Poon, and P. Duwez, Phys. Rev. B **11**, 150 (1975).
[5] Z. Altounian and J. O. Strom-Olsen, Phys. Rev. B **27**, 4149 (1983).
[6] M. Sabouri-Ghomi and Z. Altounian, J. Non-Cryst. Solids **205-207**, 692 (1996).
[7] M. L. Trudeau and R. W. Cochrane, Phys. Rev. B **41**, 10535 (1990).
[8] R. Ristić, Z. Marohnić, and E. Babić, Mater. Sci. Eng., A **226-228**, 1060 (1997).
[9] F. Hamed, F. S. Razavi, S. K. Bose, and T. Startseva, Phys. Rev. B **52**, 9674 (1995).
[10] M. Flodin, L. Hedman, and O. Rapp, Phys. Rev. B **34**, 4558 (1986).
[11] M. G. Karkut and R. R. Hake, Phys. Rev. B **28**, 1396 (1983).
[12] W. L. Johnson, S. J. Poon, J. Durand, and P. Duwez, Phys. Rev. B **18**, 206 (1978).
[13] E. R. Domb and W. L. Johnson, J. Low Temp. Phys. **33**, 29 (1978).
[14] N. R. Werthamer, E. Helfand, and P. C. Hohenberg, Phys. Rev. **147**, 295 (1966).
[15] K. Maki, Phys. Rev. **148**, 362 (1966).
[16] W. L. Carter, S. J. Poon, G. W. Hull, and T. H. Geballe, Solid State Commun. **39**, 41 (1981).
[17] S. J. Poon, Phys. Rev. B **25**, 1977 (1982).
[18] S. J. Poon, Phys. Rev. B **27**, 5519 (1983).

[19] S. J. Poon, S. K. Hasanain, and K. M. Wong, Phys. Lett. **93**, 495 (1983).
[20] Z. Altounian, S. V. Dantu, and M. Dikeakos, Phys. Rev. B **49**, 8621 (1994).
[21] M. Dikeakos, Z. Altounian, D. H. Ryan, and S. J. Kwon, J. Non-Cryst. Solids **250-252**, 637 (1999).
[22] M. Hilke, S. Reid, R. Gagnon, and Z. Altounian, Phys. Rev. Lett. **91**, 127004 (2003).
[23] J. Lefebvre, M. Hilke, R. Gagnon, and Z. Altounian, Phys. Rev. B **74**, 174509 (2006).
[24] J. Lefebvre, M. Hilke, and Z. Altounian, Phys. Rev. B **78**, 134506 (2008).
[25] R. Brüning, Z. Altounian, and J. O. Ström-Olsen, J. Appl. Phys. **62**, 3633 (1987).
[26] M. Mao and Z. Altounian, J. Non-Cryst. Solids **205-207**, 633 (1996).
[27] Y. Yamada, Y. Itoh, and U. Mizutani, Mater. Sci. Eng. **99**, 289 (1988).
[28] R. James, *Optical Principles of the Diffraction of X-Rays* (Cornell University Press, Ithaca, NY, 1962).
[29] R. Sabet-Sharghi, Z. Altounian, and W. B. Muir, J. Appl. Phys. **75**, 4438 (1994).
[30] R. Wang, Nature (London) **278**, 700 (1979).
[31] C. McKamey, D. M. Kroeger, D. S. Easton, and J. O. Scarbrough, J. Mater. Sci. **21**, 3863 (1986).
[32] J. Lefebvre, M. Hilke, Z. Altounian, K. W. West, and L. N. Pfeiffer, Phys. Rev. B **79**, 184524 (2009).
[33] P. Oelhafen, E. Hauser, and H.-J. Güntherodt, Solid State Commun. **35**, 1017 (1980).
[34] A. M. Clogston, Phys. Rev. Lett. **9**, 266 (1962).
[35] S. J. Poon, Phys. Rev. B **27**, 5519 (1983).
[36] L. P. Gor'kov, Sov. Phys. JETP **9**, 1364 (1959).
[37] L. P. Gor'kov, Sov. Phys. JETP **10**, 998 (1960).
[38] P. H. Kes and C. C. Tsuei, Phys. Rev. B **28**, 5126 (1983).
[39] W. L. McMillan, Phys. Rev. **167**, 331 (1968).
[40] S. J. Poon and P. L. Dunn, J. Low Temp. Phys. **54**, 81 (1984).
[41] Y. Liu, H. Luo, X. Leng, Z. H. Wang, L. Qiu, S. Y. Ding, and L. Z. Lin, Phys. Rev. B **66**, 144510 (2002).
[42] X. B. Xu, H. Fangohr, S. Y. Ding, M. Gu, T. B. Tang, Z. H. Han, D. Q. Shi, and S. X. Dou, Phys. Rev. B **75**, 224507 (2007).
[43] L. Ji, M. S. Rzchowski, N. Anand, and M. Tinkham, Phys. Rev. B **47**, 470 (1993).
[44] A. Kiliç, K. Kiliç, H. Yetis, and O. Çetin, New J. Phys. **7**, 212 (2005).
[45] C. A. M. dos Santos, M. S. da Luz, B. Ferreira, and A. J. S. Machado, Physica C **391**, 345 (2003).
[46] J. Lefebvre, Ph. D. thesis, McGill University, Montréal, Canada, 2008.
[47] The dirtiness parameter is usually computed from the ratio of the BCS coherence length ξ_0 to the mean free path. However, we use the experimentally determined $\xi_G(0)$ because it represents the real coherence length of our samples with consideration for the short mean-free path in the dirty limit.